Distortion in a 7xxx Aluminum Alloy during Liquid Phase Sintering

X.N. YUAN, S.H. HUO, G.B. SCHAFFER, and M. QIAN

The distortion in a sintered 7xxx aluminum alloy, Al-7Zn-2.5Mg-1Cu (wt. pct), has been investigated by sintering three rectangular bars in each batch at 893 K (620 °C) for 0 to 40 minutes in nitrogen, followed by air or furnace cooling. They were placed parallel to each other, equally spaced apart at 2 mm, with their long axes being perpendicular to the incoming nitrogen flow. Pore evolution in each sample during isothermal sintering was examined metallographically. The compositional changes across sample mid-cross section and surface layers were analyzed using energy dispersive X-ray spectroscopy and X-ray photoelectron spectroscopy depth profiling, respectively. The two outer samples bent toward the middle one, while the middle sample was essentially distortion free after sintering. The distortion in the outer samples was a result of differential shrinkage between their outer and inner surfaces during isothermal sintering. The porous outer surface showed an enrichment of oxygen around the large pores as well as lower magnesium and zinc contents than the interior and inner surface of the same sample, while the inner surface was distinguished by the presence of AlN. The differential shrinkage was caused by different oxygen contents in local sintering atmosphere and unbalanced loss of magnesium and zinc between the outer and inner surfaces.

I. INTRODUCTION

POWDER metallurgy (PM) Al parts are mostly fabricated by liquid-phase sintering (LPS).[1,2] For PM Al parts to compete with Al castings, the near-net shape attributes of PM must be conserved while satisfying the required mechanical performance. This requires strict control of distortion during the sintering process.

Many PM parts distort during LPS.[1,3] This is affected by a variety of factors including inhomogeneous green density distribution,[4,5] large density difference between the liquid phase and solid phase,[6,7] uneven temperature distribution in parts during sintering,[8] and cooling rates from the sintering temperature.[5] On the other hand, factors such as a high liquid fraction or the use of a fast heating rate may not always cause distortion. For instance, W-Cu alloys showed negligible distortion with liquid volume fractions up to 0.80;[9] varying the heating rate from 1 K/min to 15 K/min (1 °C/min to 15 °C/min) had little effect on the distor-

tion in W-Ni-Fe alloys.[10] Initial porosity and pore size had no observable effect on the distortion in 80W-16Ni-4Cu alloy.[11] These examples indicate that distortion is complex and alloy dependent.

PM Al parts are commercially sintered in nitrogen or nitrogen-rich atmospheres because nitrogen is known to enhance the sintering of Al alloys.[12–14] Previous studies on PM Al-Zn-Mg-Cu alloys have largely focused on understanding the sintering behavior,[15,16] effect of trace elements,[17,18] microstructure evolution, and mechanical properties.[19–21] Only one report[5] discussed the distortion in an Al-8Zn-2.5Mg-1Cu-0.07Pb alloy during LPS, due to the inhomogeneous green density distribution and differential shrinkage during solidification of the sintering liquid phase. The current study presents a detailed investigation of the effect of sample position on the distortion in an Al-Zn-Mg-Cu alloy during LPS in flowing nitrogen.

II. EXPERIMENTAL PROCEDURE

Rectangular bars of Al-7Zn-2.5Mg-1Cu alloy (in wt pct) were fabricated from elemental powders in a conventional press-and-sinter PM process. The experimental materials and procedures for the preparation of green samples were similar to those reported in Reference 22. Isothermal sintering was carried out at 893 K (620 °C) for 0 to 40 minutes, followed by air or furnace cooling by switching off the power. Nitrogen gas with >99.5 pct purity and <100 ppm of oxygen was used as a sintering atmosphere throughout each sintering cycle. Three rectangular bars each measuring ~56 mm × 10 mm × 4.5 mm were sintered in each batch. They were placed

X.N. YUAN, Ph.D. Candidate, and M. QIAN, Reader, are with the CAST-CRC, School of Mechanical and Mining Engineering, The University of Queensland, Brisbane, QLD 4072, Australia. Contact e-mail: ma.qian@uq.edu.au S.H. HUO, formerly Senior Research Fellow with the CAST-CRC, School of Mechanical and Mining Engineering, The University of Queensland, is now Vice President with the ECKA Granules/SCM Metal Products, Research Triangle Park, Raleigh, NC. G.B. SCHAFFER, Professor, is with the Faculty of Engineering, Architecture and Information Technology, The University of Queensland.
Manuscript submitted March 3, 2013.
Article published online September 25, 2013.

parallel to each other in the furnace, 2 mm apart, with the long axis being perpendicular to the incoming gas flow.

The sintered density was measured using the Archimedes method from oil-impregnated samples. Metallographic samples were cut through the mid-cross section of each sintered rectangular bar, followed by grinding and polishing. They were left unetched and examined using a Polyvar optical microscope (Leica Microsystems GmbH, Wetzlar, Germany) and a JEOL 6460L scanning electron microscope (SEM) (JEOL Ltd., Tokyo, Japan) equipped with a back-scattered electron detector.

X-ray photoelectron spectroscopy (XPS) analyses were conducted using a Kratos AXIS ULTRA spectrometer (Kratos Analytical Ltd., Manchester, UK) with a monochromatized Al K_α X-ray source (1486.6 eV), operated at 15 kV and 10 mA. Data collection from the exposed sample surfaces consisted of an initial survey scan ranging from 0 to 1200 eV and a series of subsequent high resolution scans which focused on characteristic peaks of Al, Mg, and N. XPS depth profiling was carried out using a 4 keV Ar^+ beam sputtering at ~2 nm/min.

III. RESULTS

A. Sintered Density and Weight Change

Figure 1(a) shows the density of each batch of samples after sintering at 893 K (620 °C) for different times, followed by air or furnace cooling. The density decreased markedly from a green density of ~93 pct theoretical density (TD) to ~80 pct TD on reaching 893 K (620 °C), an indication that substantial expansion occurred during heating to isothermal sintering temperature. The density increased steadily with increasing sintering time and achieved ~95 pct TD after 40 minutes of isothermal hold. Furnace-cooled samples showed slightly higher densities than air-cooled samples. In addition, the middle sample in each batch always had the highest sintered density, while Sample 1, which faced the incoming nitrogen flow, always showed the lowest sintered density irrespective of isothermal hold time and subsequent cooling process.

The weight change of each batch of samples is shown in Figure 1(b). All three samples experienced weight loss after 20 minutes of isothermal sintering at 893 K (620 °C). Sample 1 which faced the incoming nitrogen flow showed the greatest weight loss. The middle sample, i.e., Sample 2, consistently registered the least weight loss. Furnace-cooled samples showed slightly greater weight loss than air-cooled ones after 40 minutes of isothermal sintering at 893 K (620 °C), especially for the two outer samples.

B. Distortion

Figure 2 shows a top views of the six batches of samples shown in Figure 1. The two outer samples showed minor distortion during the first 10 minutes of isothermal hold at 893 K (620 °C). However, distortion in each outer sample intensified with increasing isother-
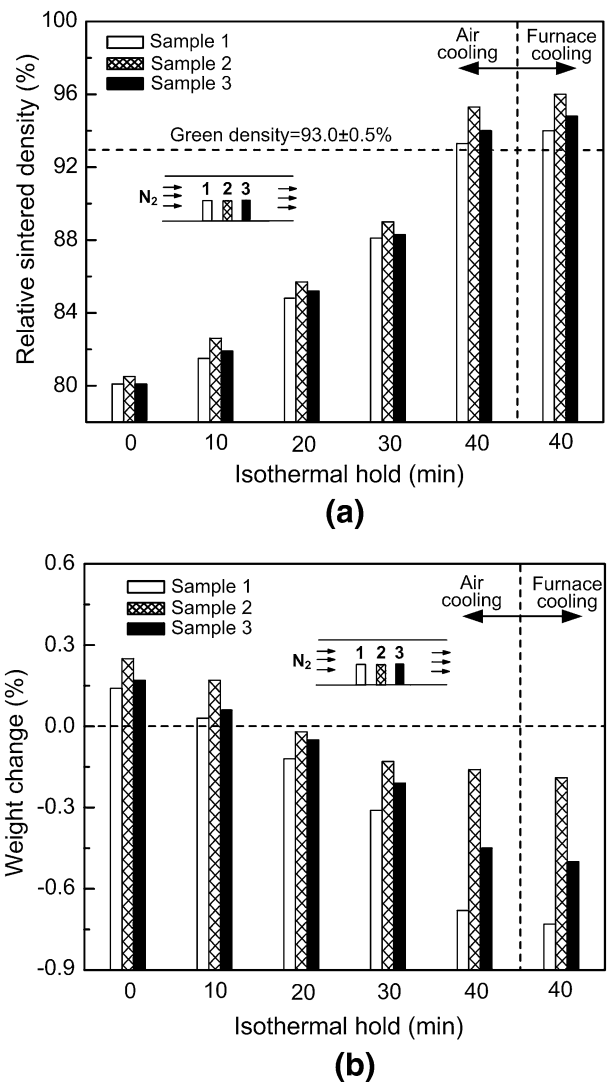

Fig. 1—(a) Density and (b) weight change of each batch of samples sintered at 893 K (620 °C) for different isothermal holds, followed by air or furnace cooling. Three samples are numbered along the incoming gas flow direction.

mal hold, and both samples bent toward the middle one. Samples cooled in the furnace after 40 minutes of isothermal sintering showed similar distortion to those cooled in air. Among all the six batches, the middle sample showed little distortion irrespective of isothermal hold and subsequent cooling process. Together with the density change of three samples during sintering shown in Figure 1(a), it is clear that the distortion was caused by sintering shrinkage during isothermal sintering, rather than the expansion during heating or the shrinkage during cooling.

C. Pore Evolution during Sintering

Figure 3 shows the pore evolution across the mid-cross section of each sample during isothermal sintering at 893 K (620 °C). The following observations are noteworthy.
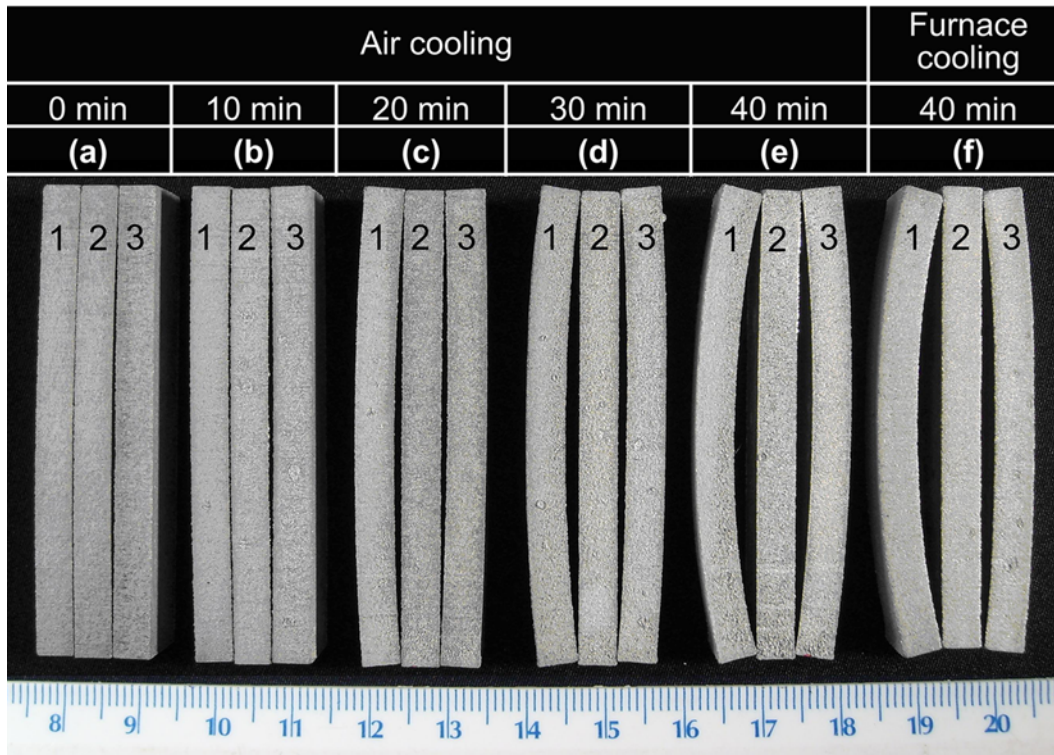
Fig. 2—A top view of six batches of samples after sintering in nitrogen at 893 K (620 °C) for 0 to 40 min. Three samples were sintered in each batch, placed perpendicular to the incoming nitrogen flow (left to right in this image) and separated by 2 mm.

- Figures 3(a) and (b)—Pores were evenly distributed throughout the mid-cross section of each sample in the first 10 minutes at 893 K (620 °C). The four edges of each section remained essentially straight.
- Figures 3(c) and (d)—Pores started to diminish and fewer pores existed in the central region of each sample. However, the pore densities on the outer and top surfaces of each sample were greater than those on the inner and bottom surfaces. This trend continued to develop with increasing isothermal hold time.
- Figures 3(d) and (e)—After 40 minutes of sintering at 893 K (620 °C), the interior of furnace-cooled samples showed fewer and smaller pores than that of air-cooled samples, although the outer surfaces had similar pore densities.

D. Microstructure

Figure 4 displays the microstructure of an Al-7Zn-2.5Mg-1Cu green sample compacted at 200 MPa, the initial state before to heating. Figure 5 shows the microstructural evolution in selected samples under different sintering conditions, where Figures $5(a_1)$ through (a_4), (d_1) through (d_4), and (e_1) through (e_4) correspond to the areas of a_1 through a_4 in Figure 3(a), d_1 through d_4 in Figure 3(d), and e_1 through e_4 in Figure 3(e), respectively.

Large and irregular pores were observed across the mid-cross section of Sample 1 on reaching 893 K (620 °C) (Figures $5(a_1)$ through (a_4)). After 40 minutes of isothermal sintering at 893 K (620 °C) and subsequent air cooling, large and irregular pores remained in the outer regions of each sample (Figure $5(d_1)$), while regions d_2, d_3, and d_4 showed much smaller pores. Solidified liquid rich in alloying elements and precipitates (bright contrast) were observed between the particle–particle boundaries. Furnace cooling resulted in microstructures (Figures $5(e_1)$ through (e_4)) similar to those in Figures $5(d_1)$ through (d_4) with the exception of a noticeable presence of precipitates. These precipitates were uniformly distributed in regions e_2 through e_4 both along the grain boundaries and inside the grains. The outer surface region e_1 showed fewer precipitates than regions e_2 through e_4.

E. Compositional Distribution

The compositional profiles across the mid-cross section of Sample 1 in Figure 3(e) after sintering at 893 K (620 °C) for 40 minutes and subsequent furnace cooling are shown in Figure 6. Three alloying elements were homogeneously distributed across the section except that the outer surface region was relatively low in Zn and Mg.

Figure 7 displays qualitative X-ray elemental mappings of O, Al, and Mg in region e_1 of Sample 1 shown in Figure 5. The sample was sintered at 893 K (620 °C) for 40 minutes, followed by furnace cooling. O and Mg were found to accumulate around the giant pores in the outer porous region e_1.
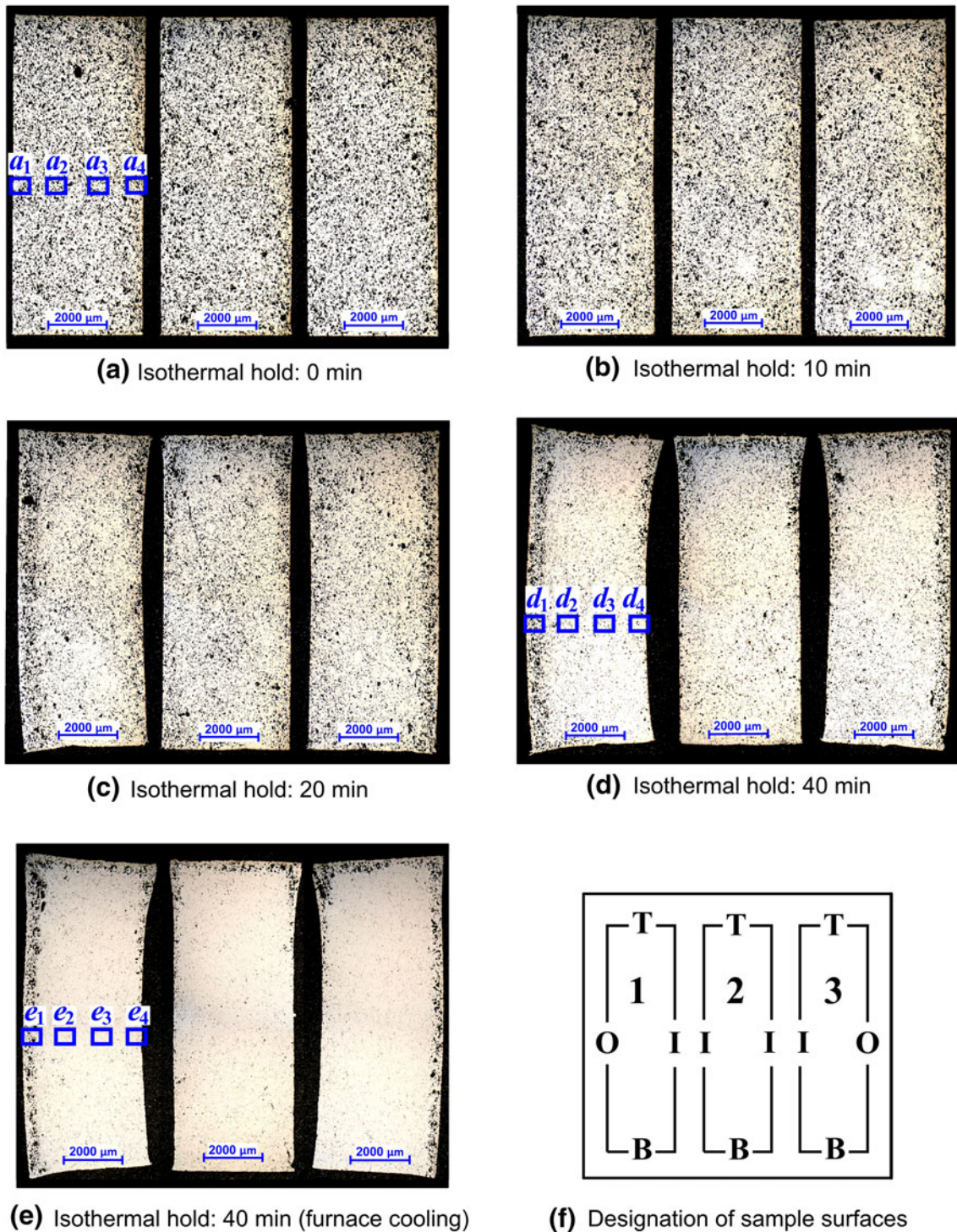
Fig. 3—Pore distribution in the mid-cross section of each sample after sintering at 893 K (620 °C) for 0 to 40 min followed by (*a*) through (*d*) air cooling or (*e*) furnace cooling. (*f*) Designation of sample surfaces: O, T, I, and B represent the outer, top, inner, and bottom surfaces, respectively.

Figure 8(a) shows the XPS depth profiles into the outer surface of Sample 1 in Figure 2(f) after sintering at 893 K (620 °C) for 40 minutes and subsequent furnace cooling. See Figure 3(f) for the designation of outer surface. Only O, Mg, C, and Al were detected by the survey scans within the sputter depth on the outer surface. The unsputtered outer surface had a significantly higher C content than the sputtered surfaces, because of carbon contamination and the residual lubricant (Acrawax C) in the sample. All sputtered outer surfaces showed a similar composition with higher O and Mg contents and a lower C content than the unsputtered surface.

The inner surface (see Figure 3(f) for the designation of inner surface) of Sample 1 in Figure 2(f) exhibited a totally different compositional depth profile from the

outer surface. The results are shown in Figure 8(b). The unsputtered inner surface had a similar composition to that of the unsputtered outer surface except for a lower Mg content. However, with increasing sputtering depth, Al content increased markedly accompanied by a rapid decrease in Mg and O contents. In addition, three extra elements–N, Cu, and Zn—were detected, with N being detected at a sputter depth of 10 nm and Cu and Zn being detected at a sputter depth of 30 nm.

Figure 9 shows high-resolution Al2p spectra obtained from the sputtered inner surface of Sample 1 in Figure 2(f). See Figure 3(f) for the designation of inner surface. Three chemical states of Al were detected corresponding to binding energies (BEs) of 72.9, 73.4,

and 74.7 eV, respectively. The intensity of the first two subpeaks increased with the increasing sputtering depth while the third subpeak decayed. These three subpeaks were identified to be metallic Al (72.9 eV),[23] Al-N bond (73.4 eV),[23–25] and Al-O bond (74.7 eV),[23,25] respectively. A high-resolution XPS scan of N1s (Figure 10) exhibited only one peak corresponding to a BE of 397.3 eV, which is consistent with the reported values for AlN.[23,24,26] A high-resolution scan of Mg2p revealed the existence of the Mg-O bond with a BE of
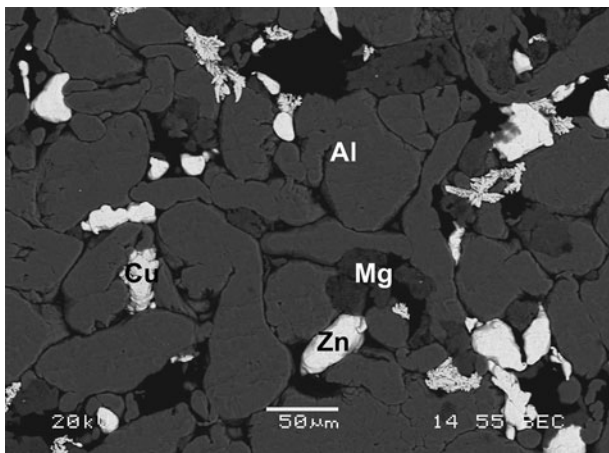

Fig. 4—Backscattered SEM micrograph of an Al-7Zn-2.5Mg-1Cu green sample compacted at 200 MPa.
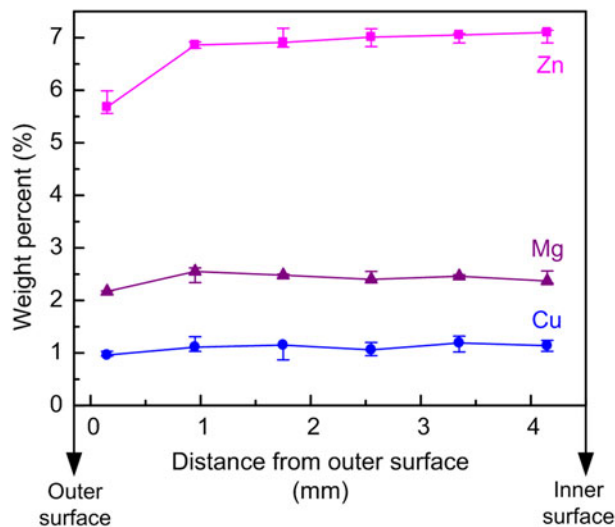

Fig. 6—Compositional profiles by EDX analysis across the mid-cross section of Sample 1 (Fig. 3(e)) after sintering at 893 K (620 °C) for 40 min and subsequent furnace cooling. See Fig. 3(f) for the designation of sample outer and inner surfaces.
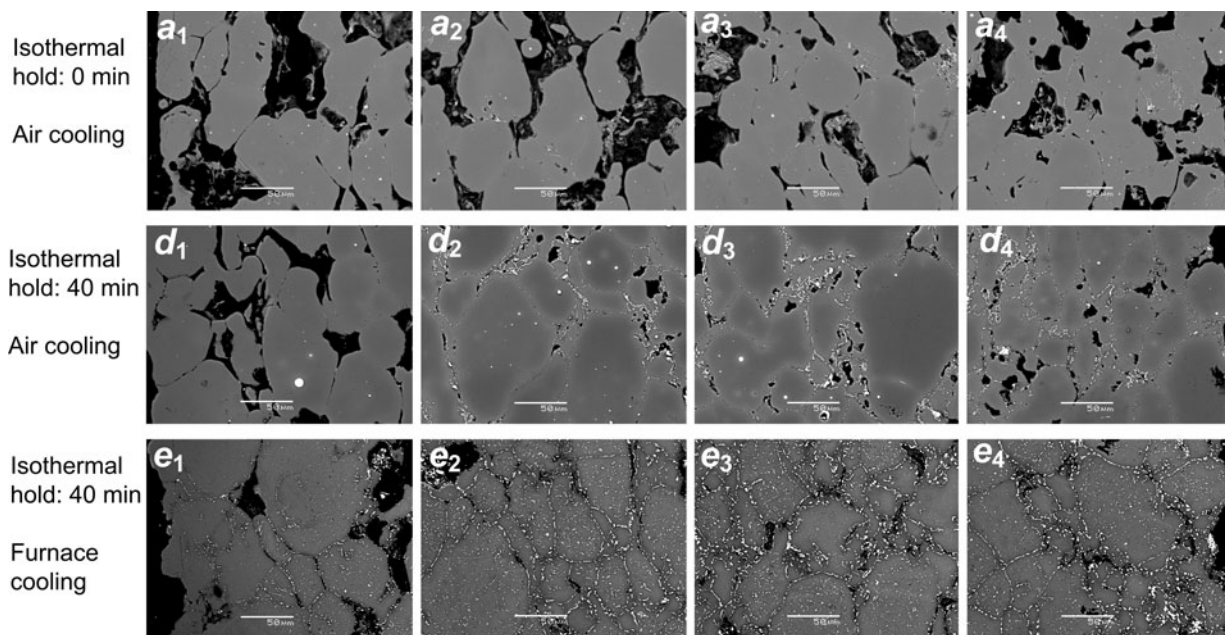

Fig. 5—Backscattered SEM micrographs of different regions in Sample 1 (Fig. 3) sintered under different conditions. (a_1 through a_4): 0 min at 893 K (620 °C) followed by air cooling; (d_1 through d_4): 40 min at 893 K (620 °C) followed by air cooling; (e_1 through e_4): 40 min at 893 K (620 °C) followed by furnace cooling. a_1 through a_4, d_1 through d_4, and e_1 through e_4 correspond to the areas of a_1 through a_4 in Fig. 3(a), d_1 through d_4 in Fig. 3(d), and e_1 through e_4 in Fig. 3(e), respectively.
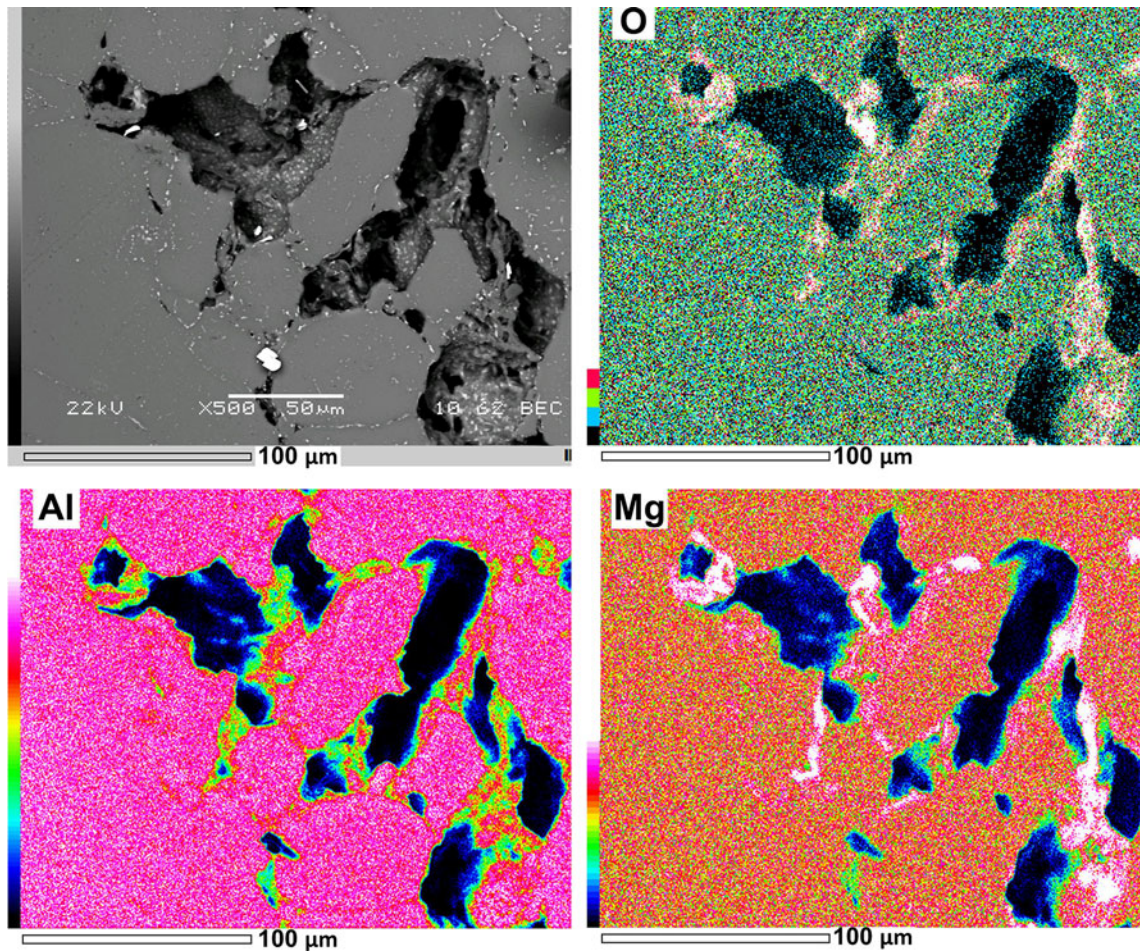
Fig. 7—SEM-EDX mappings of O, Mg, and Al in outer surface region (Fig. 5*e*1) of Sample 1 after sintering for 40 min and subsequent furnace cooling.

50.8 eV.[27] Table I summarizes the literature data on the chemical states of Al, N, and Mg.

IV. DISCUSSION

Distortion often occurs during LPS when there is a distinct difference in densities between solid and liquid or an uneven green density, or a nonuniform temperature distribution in the compact.[5,7,8] The Al-7Zn-2.5Mg-1Cu alloy studied does not contain liquid and solid phases with significantly different densities. Hence, gravity-induced distortion can be excluded. Since all samples were thin (~4.5 mm in thickness) and compacted under identical conditions, the fact that distortion was always observed in the two outer samples while the middle sample was essentially distortion immune indicates that the distortion is not related to the green density distribution. Further, a solid is isothermal if the ratio of the thermal conductivity (k_s) of the solid to that of the surrounding fluid (k_f) is greater than 1000 (k_s/k_f > 1000), and the fluid flows at a Reynolds number < 800.[28] At the sintering temperature of 893 K (620 °C), we have $k_{Al\ alloy} \approx 186$ W/mK and $k_{N2} \approx 0.0597$ W/mK.[29] This gives $k_{Al\ alloy}/k_{N2} =$

3116 ≫ 1000. In addition, the Reynolds number of the nitrogen flow in the furnace during sintering was only eight.[22] Hence, the temperature throughout each sample is expected to be uniform during isothermal sintering. The distortion observed is thus a consequence of other factors.

During heating to 893 K (620 °C), the density of each sample decreased markedly from ~93 to ~80 pct TD (Figure 1(a)) due to the expansion induced mainly by liquid formation.[17] The expansion occurred uniformly in the sample, evidenced by the negligible distortion (Figure 2(a)) before isothermal sintering at 893 K (620 °C). However, it resulted in large pores from sample surface to center (Figures 3(a), 5(a_1) through (a_4)). The microstructure was essentially uniform across the sample at this stage (Figures 5(a_1) through (a_4)). However, distinct difference in porosity developed between the center and the outer surface of Sample 1 as isothermal sintering proceeded at 893 K (620 °C), while little difference was observed between the center and the inner surface. This suggests that the flowing nitrogen over the surfaces has played a decisive role.

It has been reported that the outer layers of an Al compact serve as an oxygen getter for inner layers
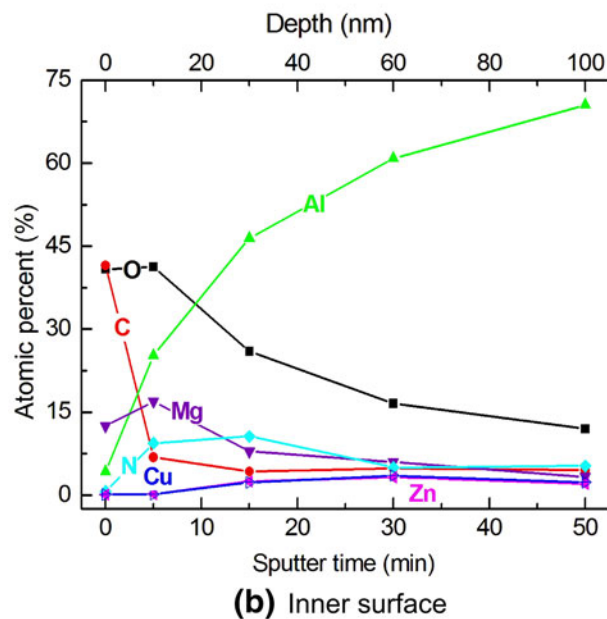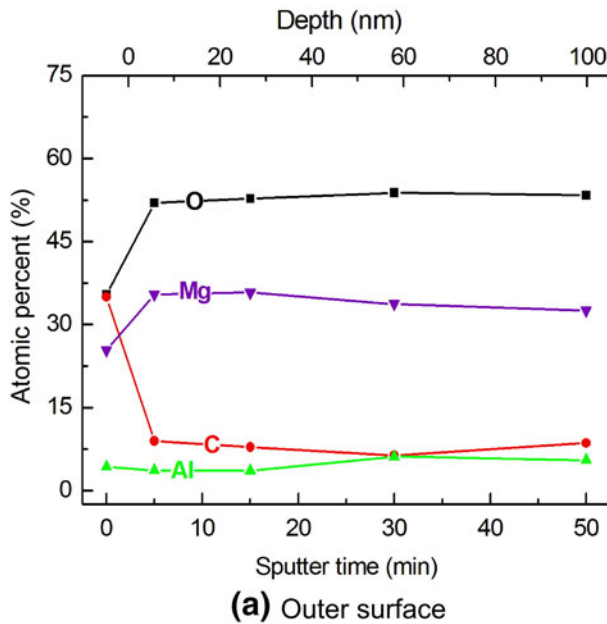
(a) Outer surface

(b) Inner surface

Fig. 8—XPS depth profiles into the outer and inner surfaces of Sample 1 in Fig. 2(f) after sintering at 893 K (620 °C) for 40 min and subsequent furnace cooling. See Fig. 3(f) for the designation of sample outer and inner surfaces.

Fig. 9—High-resolution XPS spectra of Al2p obtained from the sputtered inner surfaces of Sample 1 in Fig. 2(f) after sintering at 893 K (620 °C) for 40 min and subsequent furnace cooling. Refer to Fig. 3(f) for the designation of inner surface. Dashed traces are fitted subpeaks and indexed from low- to high- binding energy values. The solid trace is the summation of all the fitted subpeaks.

Fig. 10—High-resolution XPS spectrum of N 1 s after sputtering for 15 min obtained from the inner surface of Sample 1 in Fig. 2(f) after sintering at 893 K (620 °C) for 40 min and subsequent furnace cooling. Refer to Fig. 3(f) for the designation of inner surface.

during sintering in nitrogen, leaving a porous subsurface layer.[30] As noted previously, before the isothermal sintering at 893 K (620 °C), the density of each sample was ~80 pct TD (Figure 1(a)). In addition, the open porosity of each sample was calculated to account for ~98 pct of the total porosity following the method detailed in Reference 31. Such a high fraction of open porosity allows nitrogen gas to readily pass through the compact at the early stage of isothermal sintering. Therefore, self-gettering of oxygen is operative in the porous outer surface layers (Figures 3(a) through (e)). This is supported by the enriched O and Mg around the large pores (Figure 7) as well as the consistently high O
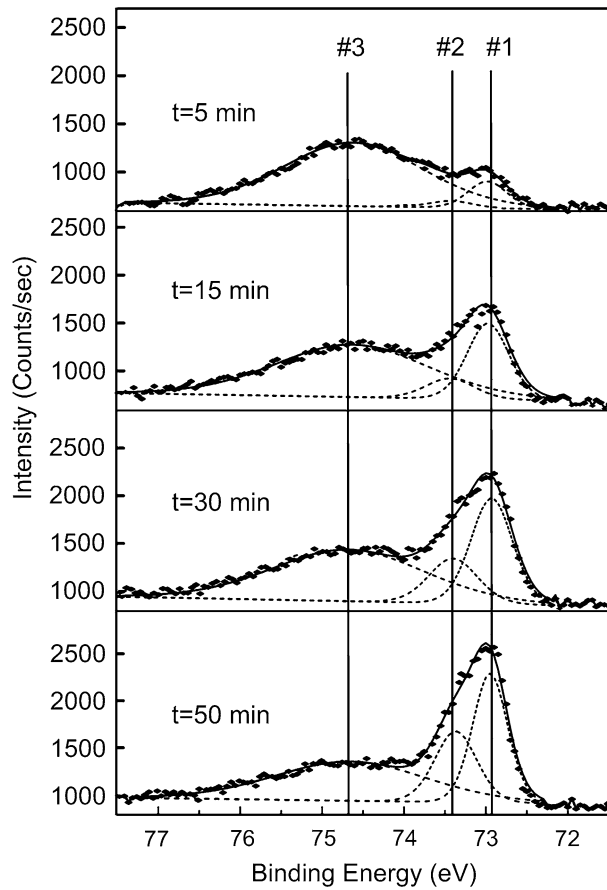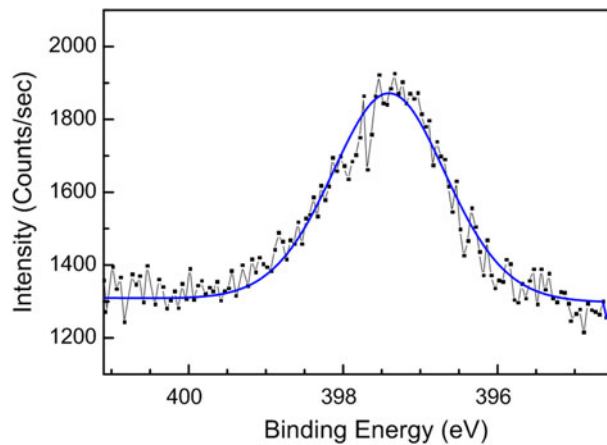
content in the outer surface layers detected by XPS (Figure 8(a)). In contrast, XPS depth profiles into the inner surfaces of Sample 1 revealed the existence of AlN

Table I. Summary of the Proposed Chemical States and Literature Data

Subpeak	Binding Energy (eV)		Chemical State
	This Work	Literature Data	
Al2p #1	72.9	72.8[23]	Metallic Al
Al2p #2	73.4	73.9,[23,24] 73.5±0.3[25]	Al-N (AlN)
Al2p #3	74.7	74.7 to 76.0,[23] 74.7±0.4[25]	Al-O (Al$_2$O$_3$)
N1s	397.3	397.2,[23,24] 397.4 ±0.2[26]	Al-N (AlN)
Mg2p	51.0	50.8[27]	Mg-O (MgO)

(Figures 8(b), 9, 10). AlN is more stable than Al$_2$O$_3$ only when $P_{O_2} < 2.66 \times 10^{-36}$ Pa in nitrogen.[32] The formation of AlN in the inner surface layers is thus indicative of a local atmosphere essentially free of oxygen. In addition, the consumption of nitrogen in the pores by the formation of AlN allows for more effective pore filling due to the reduced gas pressure.[12] This further enhances the sintering of interior and inner surface regions of Sample 1 in Figures 3(c) through (e) compared with the sintering of the outer surface layers.

Apart from the enrichment of O around pores, the outer surface (region e1 in Figure 3(e)) is also distinguished by low Zn and Mg contents (Figure 6). This is likely attributed to the evaporation of both elements which have low boiling points and high vapor pressures. Evaporations of Mg and Zn in Al alloys during heating[33–36] and resultant formation of pores in the surface layers[36,37] have been reported previously. The weight loss shown in Figure 1(b) is thus a result of the evaporations of Zn and Mg. Based on the compositional profiles shown in Figure 6, Thermo-Calc calculation predicts that the liquid fraction in the outer surface layers is about 30 pct less than in the central region. This, together with the inadequate wettability between Al$_2$O$_3$ and molten Al, leads to poorly sintered outer surface layers with a density of still ~80 pct TD, compared with the well-sintered central regions (~95 pct TD). This nonuniform shrinkage was responsible for the distortion that occurred during isothermal sintering. For similar reasons, the top surface layer and the bottom layer of each sample will sinter differently.

The distinct sintering behaviors between the outer surface and the inner surface of each outer sample shown in Figure 3 are likely to be related to the nitrogen flow behavior over the surfaces. To understand how these differences are initiated and developed, it is necessary to investigate the gas flow behavior around each sintering surface by three-dimensional (3D) computational fluid dynamics (CFD) modeling. This will be the focus of the companion paper.

V. SUMMARY

An experimental study has been made of the distortion in a sintered Al-7Zn-2.5Mg-1Cu alloy. Six batches of rectangular bars were sintered at 893 K (620 °C) for up to 40 minutes in flowing nitrogen. Each batch consisted of three samples, equally spaced 2 mm apart, placed perpendicular to the incoming nitrogen flow. The following conclusions can be drawn.

1. Significant distortion always occurred to the two outer samples, both of which bent inward toward the middle sample. In contrast, the middle sample was essentially distortion free after 40 minutes isothermal sintering at 893 K (620 °C).
2. The distortion occurred as a result of differential shrinkage between the outer and inner surfaces during isothermal sintering rather than during heating or cooling. Samples experienced significant expansion during heating to isothermal sintering temperature with a decrease in density from 93 to 80 pct TD. Nevertheless, this expansion did not lead to any noticeable distortion in the samples.
3. The porous outer surface layer of Sample 1 after sintering for 40 minutes and subsequent furnace cooling showed an enrichment of O around the large pores and lower Zn and Mg contents than the interior and the inner surface. The differential shrinkage between the outer and inner surfaces was caused by the different oxygen contents in the local sintering atmosphere and the unbalanced evaporations of Zn and Mg during sintering.
4. The distinct sintering behaviors between the outer and inner surfaces of outer samples are likely to be related to nitrogen gas behavior around these surfaces.

REFERENCES

1. R.M. German: *Sintering Theory and Practice*, Wiley, New York, NY, 1996, pp. 484452–59.
2. G.B. Schaffer, T.B. Sercombe, and R.N. Lumley: *Mater. Chem. Phys.*, 2001, vol. 67 (1–3), pp. 85–91.
3. R.M. German: *Liquid Phase Sintering*, Plenum Press, New York, NY, 1985, p. 181.

4. G.C. Kuczynski and I. Zaplatynskyj: *Trans. TMS-AIME*, 1956, vol. 206 (2), p. 215.
5. G.B. Schaffer and S.H. Huo: *Powder Metall.*, 2000, vol. 43 (2), pp. 163–67.
6. J.L. Johnson, A. Upadhyaya, and R.M. German: *Metall. Mater. Trans. B*, 1998, vol. 29B, pp. 857–66.
7. Y.X. Wu, R.M. German, B. Marx, R. Bollina, and M. Bell: *Mater. Sci. Eng. A*, 2003, vol. 344 (1–2), pp. 158–67.
8. S.X. Zhang, M. Chandrasekaran, Q.F. Li, M.K. Ho, and M.S. Yong: *Int. J. Adv. Manuf. Technol.*, 2008, vol. 38 (3–4), pp. 278–84.
9. J.L. Johnson, J.J. Brezovsky, and R.M. German: *Metall. Mater. Trans. A*, 2005, vol. 36A, pp. 1557–65.
10. R. Bollina and R.M. German: *Int. J. Refract. Met. Hard Mater.*, 2004, vol. 22 (2–3), pp. 117–27.
11. W.W. Yi, X.P. Xu, P.H. Lu, and R.M. German: *Int. J. Refract. Met. Hard Mater.*, 2001, vol. 19 (3), pp. 149–58.
12. G.B. Schaffer, B.J. Hall, S.J. Bonner, S.H. Huo, and T.B. Sercombe: *Acta Mater.*, 2006, vol. 54 (1), pp. 131–38.
13. T. Pieczonka, T. Schubert, S. Baunack, and B. Kirback: *Mater. Sci. Eng. A*, 2008, vol. 478 (1–2), pp. 251–56.
14. G.B. Schaffer, J.Y. Yao, S.J. Bonner, E. Crossin, S.J. Pas, and A.J. Hill: *Acta Mater.*, 2008, vol. 56 (11), pp. 2615–24.
15. M. Muhlburger and P. Paschen: *Z. Metallkd.*, 1993, vol. 84, pp. 346–50.
16. J.M. Martin, T. Gomez-Acebo, and F. Castro: *Powder Metall.*, 2002, vol. 45 (2), pp. 173–80.
17. G.B. Schaffer and S.H. Huo: *Powder Metall.*, 1999, vol. 42 (3), pp. 219–26.
18. G.B. Schaffer, S.H. Huo, J. Drennan, and G.J. Auchterlonie: *Acta Mater.*, 2001, vol. 49 (14), pp. 2671–78.
19. R.N. Lumley and G.B. Schaffer: *Scripta Mater.*, 2006, vol. 55 (3), pp. 207–10.
20. M.S. Mohammadi, A. Simchi, and C. Gierl: *Powder Metall.*, 2010, vol. 53 (1), pp. 62–70.
21. A.D.P. LaDelpha, H. Neubing, and D.P. Bishop: *Mater. Sci. Eng. A*, 2009, vol. 520 (1–2), pp. 105–13.
22. X.N. Yuan, S.M. Aminossadati, S.H. Huo, G.B. Schaffer, and M. Qian: *Metall. Mater. Trans. A*, 2012, vol. 43A, pp. 4345–55.
23. W. Österle, I. Dörfel, I. Urban, T. Reier, and J.W. Schultze: *Surf. Coat. Technol.*, 1998, vol. 102, pp. 168–74.
24. D. Hoche, C. Blawert, M. Cavellier, D. Busardo, and T. Gloriant: *Appl. Surf. Sci.*, 2011, vol. 257 (13), pp. 5626–33.
25. L. Rosenberger, R. Baird, E. McCullen, G. Auner, and G. Shreve: *Surf. Interface Anal.*, 2008, vol. 40 (9), pp. 1254–61.
26. M.J. Cristobal, C.M. Abreu, R. Figueroa, G. Pena, and M.C. Perez: *Surf. Interface Anal.*, 2010, vol. 42 (6–7), pp. 592–96.
27. H.B. Yao, Y. Li, and A.T.S. Wee: *Appl. Surf. Sci.*, 2000, vol. 158 (1–2), pp. 112–19.
28. T.J. Young and K. Vafai: *Int. J. Heat Mass Transf.*, 1998, vol. 41 (21), pp. 3279–98.
29. F.P. Incropera, D.P. Dewitt, T.L. Bergman, and A.S. Lavine: *Fundamentals of Heat and Mass Transfer*, 6th ed., Wiley, New York, NY, 2007, p. 929, 944.
30. G.B. Schaffer and B.J. Hall: *Metall. Mater. Trans. A*, 2002, vol. 33A, pp. 3279–84.
31. P. Yu, M. Yan, G.B. Schaffer, and M. Qian: *Metall. Mater. Trans. A*, 2011, vol. 42A, pp. 2040–47.
32. M. Qian and G.B. Schaffer: in *Sintering of Advanced Materials*, Z.Z. Fang, ed., Woodhead Publishing Limited, Cambridge, U.K., 2010, pp. 289–322.
33. F. Czerwinski: *Corros. Sci.*, 2004, vol. 46 (2), pp. 377–86.
34. F.J. Esposto, C.S. Zhang, P.R. Norton, and R.S. Timsit: *Surf. Sci.*, 1994, vol. 302 (1–2), pp. 109–20.
35. A. Kimura, K. Kondoh, M. Shibata, and R. Watanabe: *Mater. Trans. JIM*, 2001, vol. 42 (7), pp. 1373–79.
36. S.Z. Bokshtein, D.A. Giunashvili, T.I. Gudkova, and S.T. Kishkin: *Met. Sci. Heat Treat.*, 1967, vol. 8 (8), pp. 603–606.
37. K.G.E. Brenner and O.K. Demel: *J. Phys. F*, 1975, vol. 5 (11), pp. 2026–34.